J. Fluid Mech. (1988), *vol.* 188, *pp.* 571–583
Printed in Great Britain

A model for the onset of penetrative convection

By P. C. MATTHEWS

Department of Applied Mathematics and Theoretical Physics, University of Cambridge, Silver Street, Cambridge CB3 9EW, UK

(Received 14 February 1987 and in revised form 17 August 1987)

The stability of an S-shaped, cubic temperature profile, maintained by internal heating, is considered as a model for circumstances in which an unstably stratified layer of fluid is bounded by two stable layers. Critical Rayleigh numbers are computed for the cases of an infinitely deep layer, and for a layer of finite depth with symmetrically placed free or rigid boundaries. It is found that the introduction of boundaries can reduce the stability of the system. A weakly nonlinear analysis shows that the bifurcation is supercritical and that rolls are preferred to squares for all values of the Prandtl number. This result prompts a re-examination of the model of penetrative convection in water above ice, in which the bifurcation is subcritical, in order to understand the difference between the two models.

1. Introduction

In many problems in geophysical fluid dynamics, convection occurs when an unstably stratified layer of fluid is bounded by two stably stratified layers. As a model for the onset of this form of penetrative convection, the stability of a cubic density profile may be analysed (figure 1). The density profile is assumed to be caused by a cubic temperature profile, maintained by an internal heat source.

This work was prompted by consideration of an ice-covered lake subjected to solar heating. The upper layers of the lake are warmed, and so increase in density if the temperature is below 4 °C, but the upper surface of the water is maintained at 0 °C by the ice. If the initial temperature profile is linear, solution of the diffusion equation with the appropriate internal heating leads to a density profile qualitatively similar to that of figure 1 with the temperature profile reversed (Matthews & Heaney 1987).

Penetrative convection is however a widely occurring phenomenon. For example, in stars convection below the surface overshoots into the stably stratified surface layer, causing the granulation pattern observed on the surface of the sun. Penetrative convection also occurs in the ocean and in lakes, when the surface is cooled at night, where the penetration of the mixed layer into the stable region below is important for thermocline formation. It also occurs in the atmosphere, when the ground is warmed by the sun; and may take place in the Earth's mantle, where internal heating is provided by radioactive decay.

Despite all these physical applications, penetrative convection has not received much theoretical attention compared with Rayleigh–Bénard convection. The one model which has been discussed extensively is the 'ice–water' model, first proposed by Malkus (1960) and analysed by Veronis (1963). In this model, a layer of water has a linear temperature profile around 4 °C. Because of the quadratic equation of state of water near 4°, the density profile is parabolic, the water below the 4° isotherm being unstable. Veronis (1963) showed that the bifurcation at the critical Rayleigh

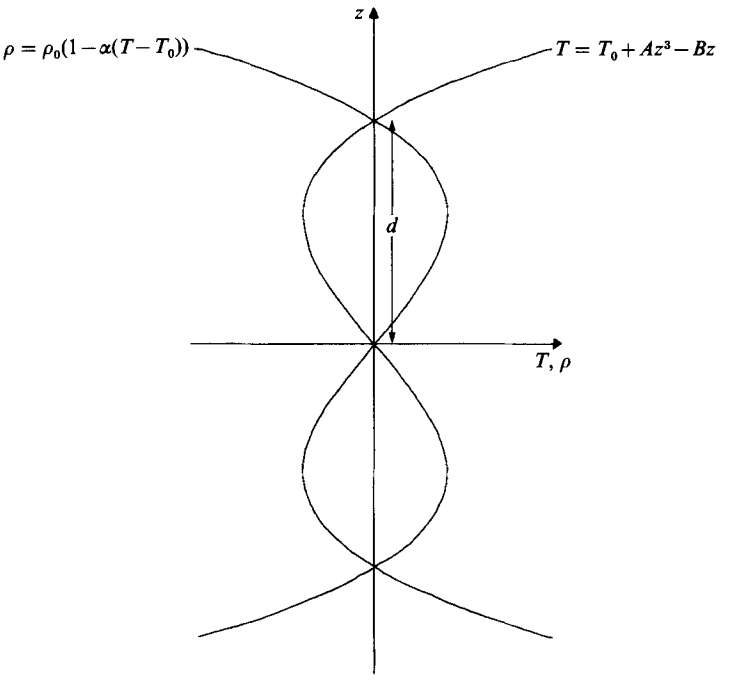

FIGURE 1. The temperature and density profiles under consideration, showing the lengthscale used for non-dimensionalization.

number for this problem is subcritical, and the associated hysteresis effect as the Rayleigh number is raised and lowered has been observed experimentally by Azouni (1983). The subcritical bifurcation means that weakly nonlinear analysis around the critical Rayleigh number can only predict behaviour on an unstable solution branch, and hence cannot predict the chosen planform for convection.

2. Formulation of the problem

Consider a layer of a Boussinesq fluid, with a constant expansion coefficient α and a temperature profile

$$T(z) = T_0 + Az^3 - Bz, \tag{2.1}$$

where A and B are positive constants. To maintain this temperature profile we require an internal heat source, $H(z) = -6KAz$, where K is the thermal diffusivity. (For the case of an ice-covered lake, A, B and α are negative. The solar heat source declines exponentially, but a linear heat source can capture the essential shape of the temperature profile.) Non-dimensionalizing with $d = (B/A)^{\frac{1}{2}}$ as a lengthscale and Bd as a temperature scale, and introducing a perturbation temperature θ, the equations for momentum and heat transport become

$$\frac{1}{\sigma}\left(\frac{\partial \boldsymbol{u}}{\partial t} + \boldsymbol{u}\cdot\nabla\boldsymbol{u}\right) = -\nabla P + R\theta\hat{\boldsymbol{z}} + \nabla^2\boldsymbol{u}, \tag{2.2}$$

$$\frac{\partial\theta}{\partial t} + \boldsymbol{u}\cdot\nabla(z^3 - z + \theta) = \nabla^2\theta, \tag{2.3}$$

where $\sigma = \nu/K$ is the Prandtl number and R is the Rayleigh number given by

$$R = \frac{g\alpha B d^4}{\nu K}. \tag{2.4}$$

3. The linear stability problem

The linearized forms of (2.2) and (2.3) are

$$\frac{1}{\sigma}\frac{\partial \boldsymbol{u}}{\partial t} = -\nabla P + R\theta\hat{\boldsymbol{z}} + \nabla^2 \boldsymbol{u}, \tag{3.1}$$

$$\frac{\partial \theta}{\partial t} = \boldsymbol{u}\cdot\hat{\boldsymbol{z}}(1-3z^2) + \nabla^2\theta. \tag{3.2}$$

Since it can be shown that there is no vertical vorticity, $\boldsymbol{u}$ may be represented as $\boldsymbol{u} = (u, v, w) = \nabla\times\nabla\times(\phi\hat{\boldsymbol{z}})$. Setting $\phi = h(x,y)f(z)\,e^{st}$, $\theta = h(x,y)\,g(z)\,e^{st}$ and taking $\hat{\boldsymbol{z}}\cdot\nabla\times\nabla\times$ (3.1) we obtain

$$\nabla_{\mathrm{H}}^2 h = -k^2 h, \tag{3.3}$$

$$\frac{s}{\sigma}(\mathrm{D}^2-k^2)f = -Rg + (\mathrm{D}^2-k^2)^2 f, \tag{3.4}$$

$$sg = k^2 f(1-3z^2) + (\mathrm{D}^2-k^2)g, \tag{3.5}$$

where k is the horizontal wavenumber of the disturbance, $\mathrm{D}^2 = \mathrm{d}^2/\mathrm{d}z^2$ and ∇_{H}^2 is the horizontal Laplacian. Eliminating g leads to

$$(\mathrm{D}^2-k^2)(\mathrm{D}^2-k^2-s)\left(\mathrm{D}^2-k^2-\frac{s}{\sigma}\right)f + Rk^2(1-3z^2)f = 0. \tag{3.6}$$

It can be shown (Veronis 1963) that s is real for a growing or neutral mode ($\mathrm{Re}\,(s) \geqslant 0$), in the case of an unbounded region of fluid or with stress-free boundaries, but this principle of exchange of stabilities cannot be proved for rigid boundaries. If it does hold, we can set $s = 0$ to examine the onset of instability. The eigenvalue problem for $R_0(k)$ is then

$$(\mathrm{D}^2-k^2)^3 f + R_0 k^2(1-3z^2)f = 0, \tag{3.7}$$

where the subscript 0 denotes that the Rayleigh number is critical.

3.1. *Unbounded case – solution by Fourier transform*

Taking the Fourier transform of (3.7) gives

$$(\omega^2+k^2)^3\hat{f}(\omega) - R_0 k^2\hat{f}(\omega) - 3R_0 k^2\frac{\mathrm{d}^2\hat{f}(\omega)}{\mathrm{d}\omega^2} = 0, \tag{3.8}$$

where

$$\hat{f}(\omega) = \int_{-\infty}^{\infty} \mathrm{e}^{-\mathrm{i}\omega z} f(z)\,\mathrm{d}z$$

is the Fourier transform of $f(z)$. The transform $\hat{f}(\omega)$ exists because $f(z)\to 0$ as $z\to\pm\infty$; similarly, for $f(z)$ to exist, $\hat{f}(\omega)$ must tend to zero at large $|\omega|$. A shooting method was used to solve for $\hat{f}(\omega)$, with the boundary conditions

$$\hat{f}(0) = \int_{-\infty}^{\infty} f(z)\,\mathrm{d}z = 1,$$

since the scaling of $f(z)$ is arbitrary, and

$$\frac{\mathrm{d}\hat{f}}{\mathrm{d}\omega}(0) = \int_{-\infty}^{\infty} -\mathrm{i}zf(z)\,\mathrm{d}z = 0,$$

since for the lowest eigenvalue we expect $f(z)$ and hence $\hat{f}(\omega)$ to be even. Equation (3.8) was integrated numerically from $\omega = 0$ using a fourth-order Runge–Kutta method, and the parameter R was varied until $\hat{f}(\omega)$ approached zero at large ω.

The function $R_0(k)$ has a single minimum which occurs at

$$k_\mathrm{c} = 1.26, \quad R_\mathrm{c} = 88.0,$$

where the subscript c denotes the minimum critical Rayleigh number and the associated wavenumber. To compare these values with those for convection between two parallel plates, we can use the depth of the unstable layer as a lengthscale, and the temperature difference across the unstable layer as our temperature scale. With this scaling, the critical values of k and R become

$$k_\mathrm{c} = 1.45, \quad R_\mathrm{c} = 104.$$

R_c is considerably less than that for Rayleigh–Bénard convection, which is 657 for stress-free boundaries and 1708 for rigid boundaries. Latour & Zahn (1978) found that for an unstable linear profile bounded by two stable linear profiles with the same density gradient,

$$k_\mathrm{c} = 1.05, \quad R_\mathrm{c} = 60.9.$$

This 'Z' profile is rather less stable than our 'S' profile, perhaps because of the sharp discontinuities in the temperature gradient of the former, or because of the rapidly increasing temperature gradient in the stable regions of the latter.

Having obtained a solution for $\hat{f}(\omega)$, the Fourier transform was inverted numerically to find $f(z)$. The results show that convection overshoots well into the stable layer, the top of the main cell being at $z = 1.69$ in our scaling. Above this there is a weak countercell, driven by viscous forces from the main cell. Figure 2 shows w, u and θ, with arbitrary scaling, and figure 3 shows the streamlines, assuming convection in the form of rolls, i.e. $h(x, y) \propto \cos(kx)$. The streamlines are plotted much more closely in the countercell than in the main cell. There is in fact a sequence of countercells, alternating in direction of rotation and becoming weaker in magnitude and shorter in depth, which can be found by asymptotic methods.

The Fourier-transform method was also used to look at the first odd solution of (3.8), corresponding to a solution with two main convection cells. This gave the results $k_\mathrm{c} = 2.91$, $R_\mathrm{c} = 3705$.

3.2. *Stress-free boundaries*

We now consider the effect of introducing stress-free, constant-temperature boundaries at $z = L$ and $z = -L$. In this case, $f(z)$ obeys (3.7) with the boundary conditions

$$f = \mathrm{D}^2 f = \mathrm{D}^4 f = 0 \quad \text{at } z = \pm L.$$

Expanding $f(z)$ as a cosine series,

$$f(z) = \sum_{n=1}^{\infty} A_n \cos\left[\frac{(n-\tfrac{1}{2})\pi z}{L}\right], \tag{3.9}$$

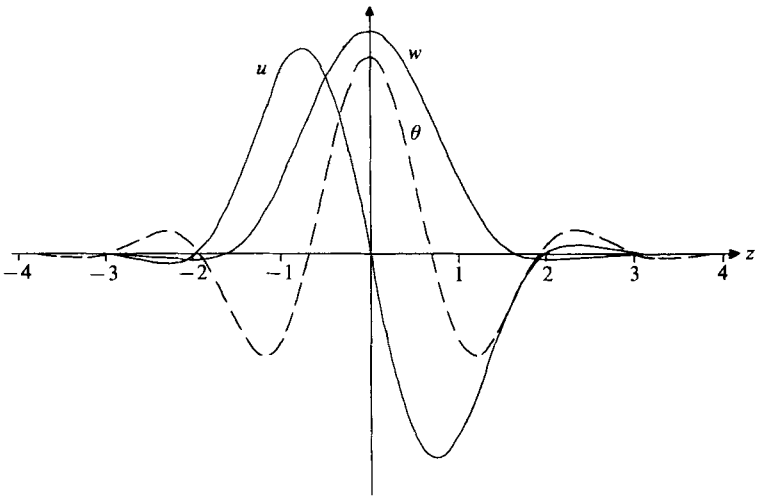

FIGURE 2. The vertical and horizontal velocity and the temperature fluctuation of the linear solution, with arbitrary scaling.

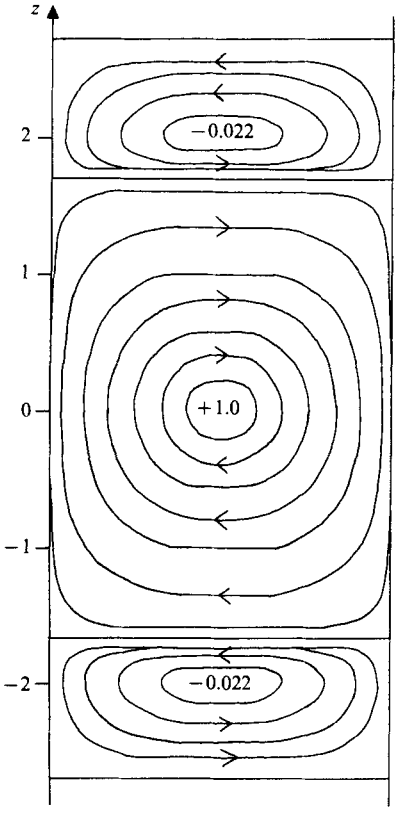

FIGURE 3. Streamlines in the main cell and first countercell, showing the stream-function values at the centre of each cell.

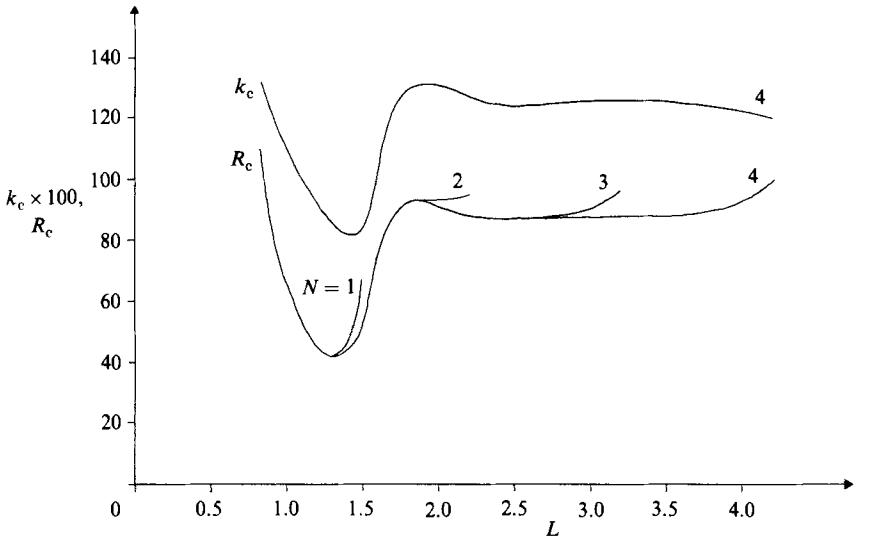

FIGURE 4. Variation of critical wavenumber and Rayleigh number with position of stress-free boundaries, using an N-term cosine series.

automatically satisfies these boundary conditions. Substituting (3.9) into (3.7), multiplying by $\cos[(m-\frac{1}{2})\pi z/L]$ and integrating from $z=-L$ to $z=L$ gives the following relationship between the A_n:

$$\left[\left\{\frac{(m-\frac{1}{2})^2\pi^2}{L^2}+k^2\right\}^3 - R_0 k^2 + R_0 k^2 L^2\left\{1-\frac{6}{(2m-1)^2\pi^2}\right\}\right]A_m + \frac{6R_0 k^2 L^2}{\pi^2}\sum_{n+m}^{\infty}\left[\frac{(-1)^{m-n}}{(m-n)^2}+\frac{(-1)^{m+n-1}}{(m+n-1)^2}\right]A_n = 0. \quad (3.10)$$

If the series is truncated at $n=N$, then (3.10) gives N homogeneous equations for the A_n, so $R_0(k)$ is given approximately by the condition that the order-N determinant vanishes.

For each value of L, k was varied until the value of R_0 found from the zero of the determinant was minimized. Figure 4 shows how R_c and k_c vary with L, and how each N-term cosine series breaks down as L increases. The maximum number of terms used was four, giving accuracy up to about $L=3.5$. The accuracy can be judged by comparison of the 3-term results with those using 4 terms, and by comparing the results at large L with those obtained for the case without boundaries: $R_c(L)$ appears to be tending to 88, and k_c to 1.26, at large L. Note that $R_c(L)$ and $k_c(L)$ are oscillatory functions. R_c has a minimum of 41.7 at $L=1.32$, less than half its asymptotic value. This effect was also found by Veronis (1963), for his penetrative convection model described in §1, but it was much less marked, the ratio of the minimum critical Rayleigh number to its asymptotic value being 0.85.

The reason why boundaries can reduce R_c is that they can cut out the regions of negative convective heat flux near the top and bottom of the main cell and in the countercells (figure 2) which reduce the efficiency of convection. The minima and maxima in figure 4 are caused by the changes in sign of w and θ as L is increased.

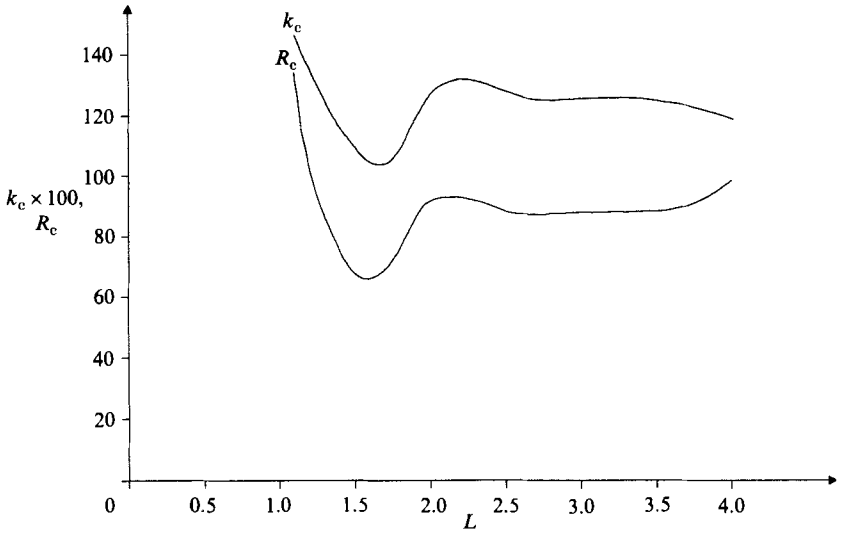

FIGURE 5. Variation of critical wavenumber and Rayleigh number with position of rigid boundaries, using a 4-term cosine series.

3.3. *Rigid boundaries*

The problem for rigid boundaries can be considered in a similar way, if the principle of exchange of stabilities is assumed. The cosine series does not satisfy the boundary conditions, which are $f = \mathrm{D}f = g = 0$ at $z = \pm L$. Since $\mathrm{D}^2 f \neq 0$ at the boundaries, the cosine series is only once differentiable and $\mathrm{D}^2 f(L)$ is an extra parameter in the problem. For this we require an extra equation, which comes from the second boundary condition:

$$\sum_{n=1}^{N} A_n (n-\tfrac{1}{2})(-1)^n = 0. \tag{3.11}$$

Figure 5 shows that the results are qualitatively similar to those for stress-free boundaries. Again $R_c(L)$ approaches 88 and $k_c(L)$ approaches 1.26 at large L. The minimum Rayleigh number is $R_c = 65.9$ at $L = 1.6$, so introducing rigid boundaries can also make the system less stable, although not to the same extent as stress-free boundaries. However the critical Rayleigh number for rigid boundaries is less than that for stress-free boundaries for $1.6 < L < 2.0$.

4. Weakly nonlinear analysis

A weakly nonlinear expansion method is now used to study the bifurcation at R_c and to compare two different planforms. The method is standard, and similar to that used by Jenkins & Proctor (1984). The variables are expanded in a power series as follows:

$$\boldsymbol{u} = \epsilon \boldsymbol{u}_1 + \epsilon^2 \boldsymbol{u}_2 + \epsilon^3 \boldsymbol{u}_3 \ldots, \quad \theta = \epsilon\theta_1 + \epsilon^2\theta_2 + \epsilon^3\theta_3 \ldots,$$

$$P = \epsilon P_1 + \epsilon^2 P_2 + \epsilon^3 P_3 \ldots, \quad R = R_c + \epsilon^2 R_2 \ldots$$

and the evolution of the system is studied on a slow timescale $\tau = \epsilon^2 t$. These expansions are substituted into the nonlinear equations (2.2) and (2.3) and powers of ϵ are equated.

At first order in ϵ the linearized equations appear, so we can set $\boldsymbol{u}_1 = \nabla \times \nabla \times$

$(\phi_1 \hat{z})$, where $\phi_1 = h(x,y)f(z)$, and $\theta_1 = h(x,y)g(z)$, where $g(z) = (1/R_c)(\mathrm{D}^2 - k^2)^2 f(z)$, from (3.4). Setting

$$h(x,y) = A_1(\tau)\cos kx + A_2(\tau)\cos ky \tag{4.1}$$

allows the possibility of convection in the form of rolls ($A_2 = 0$) or squares ($A_1 = A_2$), both of which have been shown to occur in certain physical problems (e.g. Jenkins & Proctor 1984). ϕ_1 can then be written as $\phi_{11} + \phi_{12}$ where $\phi_{11} = A_1 \cos kx f(z)$, $\phi_{12} = A_2 \cos ky f(z)$.

At second order, the equations are

$$\frac{1}{\sigma}\boldsymbol{u}_1 \cdot \boldsymbol{\nabla}\boldsymbol{u}_1 = -\boldsymbol{\nabla}P_2 + R_c\,\theta_2\,\hat{\boldsymbol{z}} + \nabla^2\boldsymbol{u}_2, \tag{4.2}$$

$$\boldsymbol{u}_1 \cdot \boldsymbol{\nabla}\theta_1 = w_2(1-3z^2) + \nabla^2\theta_2. \tag{4.3}$$

Taking $\hat{\boldsymbol{z}} \cdot \boldsymbol{\nabla} \times \boldsymbol{\nabla} \times$ (4.2) gives

$$\hat{\boldsymbol{z}} \cdot \boldsymbol{\nabla} \times \boldsymbol{\nabla} \times \left(\frac{1}{\sigma}\boldsymbol{u}_1 \cdot \boldsymbol{\nabla}\boldsymbol{u}_1\right) = -R_c\,\nabla_H^2\,\theta_2 - \nabla^4 w_2. \tag{4.4}$$

As at first order, $\boldsymbol{u}_2$ can be written as $\boldsymbol{u}_2 = \boldsymbol{\nabla} \times \boldsymbol{\nabla} \times (\phi_2 \hat{\boldsymbol{z}})$. Now the forcing terms on the left-hand sides of (4.3) and (4.4) have a horizontal dependence which suggests the following forms for ϕ_2 and θ_2:

$$\phi_2 = (A_1^2 \cos 2kx + A_2^2 \cos 2ky)\,F_2(z) + A_1 A_2 \cos kx \cos ky\, F_3(z), \tag{4.5}$$

$$\theta_2 = (A_1^2 + A_2^2)\,G_1(z) + (A_1^2 \cos 2kx + A_2^2 \cos 2ky)\,G_2(z) + A_1 A_2 \cos kx \cos ky\, G_3(z). \tag{4.6}$$

Substituting into (4.3) and (4.4) gives five differential equations for the five second-order functions, which can be solved by a shooting method, using the fact that these are all odd functions of z because the forcing terms are odd. This was done using a Runge–Kutta method, with a step length of $\frac{1}{16}$, taking each function as far as $z = 4$.

At third order in ϵ, the time dependence appears:

$$\frac{1}{\sigma}\left(\frac{\partial \boldsymbol{u}_1}{\partial \tau} + \boldsymbol{u}_1 \cdot \boldsymbol{\nabla}\boldsymbol{u}_2 + \boldsymbol{u}_2 \cdot \boldsymbol{\nabla}\boldsymbol{u}_1\right) - R_2\,\theta_1\,\hat{\boldsymbol{z}} = -\boldsymbol{\nabla}P_3 + R_c\,\theta_3\,\hat{\boldsymbol{z}} + \nabla^2\boldsymbol{u}_3, \tag{4.7}$$

$$\frac{\partial \theta_1}{\partial \tau} + \boldsymbol{u}_1 \cdot \boldsymbol{\nabla}\theta_2 + \boldsymbol{u}_2 \cdot \boldsymbol{\nabla}\theta_1 = w_3(1-3z^2) + \nabla^2\theta_3. \tag{4.8}$$

By taking $\hat{\boldsymbol{z}} \cdot \boldsymbol{\nabla} \times \boldsymbol{\nabla} \times$ (4.7) and eliminating θ_3 we obtain

$$\nabla^6 w_3 - R_c\,\nabla_H^2\,w_3(1-3z^2) = -\nabla^2(\hat{\boldsymbol{z}} \cdot \boldsymbol{\nabla} \times \boldsymbol{\nabla} \times \boldsymbol{r}_1) - R_c\,\nabla_H^2\,r_2, \tag{4.9}$$

where $\boldsymbol{r}_1$ and r_2 are the left-hand sides of (4.7) and (4.8) respectively.

The operator on the left of (4.9) is the same self-adjoint operator as occurred at first order with zero forcing. Hence by multiplying (4.9) by either of the first-order functions ϕ_{11} or ϕ_{12}, averaging in x and y and integrating in the z-direction, we can derive the two solvability conditions

$$\langle \phi_{11,12}(\nabla^2 \hat{\boldsymbol{z}} \cdot \boldsymbol{\nabla} \times \boldsymbol{\nabla} \times \boldsymbol{r}_1 + R_c\,\nabla_H^2\,r_2)\rangle = 0, \tag{4.10}$$

where $\langle\ \rangle$ denotes the horizontal average and vertical integral. Evaluation of the solvability conditions leads to the following equations for the time evolution of A_1 and A_2:

$$C\frac{\mathrm{d}A_1}{\mathrm{d}\tau} = DR_2A_1 + EA_1^3 + FA_1A_2^2, \tag{4.11a}$$

$$C\frac{\mathrm{d}A_2}{\mathrm{d}\tau} = DR_2A_2 + EA_2^3 + FA_2A_1^2, \tag{4.11b}$$

where the numbers C, D, E and F are integrals of quantities involving the first- and second-order functions.

The numbers C and D involve only the first-order functions and are always positive, so the linear parts of (4.11) simply repeat that the static solution is linearly stable for $R < R_c$. There are three other possible equilibria,

$$A_2 = 0, \quad A_1^2 = -\frac{DR_2}{E}, \tag{4.12}$$

$$A_1 = 0, \quad A_2^2 = -\frac{DR_2}{E}, \tag{4.13}$$

$$A_1^2 = A_2^2 = -\frac{DR_2}{F+E}. \tag{4.14}$$

The solutions (4.12) and (4.13) correspond to rolls, while (4.14) represents squares. If $E > 0$, then roll solutions exist for $R_2 < 0$ and the bifurcation is subcritical. If $E < 0$, the bifurcation to rolls is supercritical. For squares, the bifurcation is subcritical if $E+F > 0$ and supercritical if $E+F < 0$. Using (4.11) to analyse the stability of these solutions, it can be shown that rolls are stable if $E < 0$ and $E > F$, while squares are stable if $E+F < 0$ and $E < F$.

The constants E and F were evaluated using a Romberg integration routine, using 64 points and taking each function as far as $z = 4.0$. The results were

$$E = -\frac{0.233}{\sigma^2} - \frac{0.231}{\sigma} - 15.1, \tag{4.15}$$

$$F = -\frac{2.24}{\sigma^2} - \frac{0.153}{\sigma} - 17.3. \tag{4.16}$$

Note that these values are proportional to the fourth power of the arbitrary scaling at first order, which was chosen such that $f(0) = 1$. The calculations were repeated for the case of stress-free boundaries at $z = \pm 3.2$, expressing the second-order functions as a 4-term sine series, giving very similar results, with a difference of less than 2%.

For all values of the Prandtl number, E and F are negative and $E > F$. This means that the bifurcation at R_c is supercritical, and that rolls are preferred to squares. We cannot say that the roll planform will be selected, because we have not considered all possible planforms. It was checked that the odd solution to (3.7) also leads to a supercritical bifurcation.

5. Comparison with the Veronis model

The result that the bifurcation is supercritical in our 'S' model contrasts with that of Veronis (1963), who found a subcritical bifurcation for his model of penetrative convection. In the latter model, the equation of state is

$$\rho(T) = \rho_0(1-\beta(T-\Delta T)^2), \tag{5.1}$$

where $\Delta T = 4$ °C. Using the depth d of the unstable layer as a lengthscale and ΔT as a temperature scale, the equations analogous to (2.2) and (2.3) are

$$\frac{1}{\sigma}\left(\frac{\partial \boldsymbol{u}}{\partial t}+\boldsymbol{u}\cdot\boldsymbol{\nabla}\boldsymbol{u}\right) = -\boldsymbol{\nabla}P + R(2\theta(z-1)+\theta^2)\,\hat{\boldsymbol{z}}+\nabla^2\boldsymbol{u}, \tag{5.2}$$

$$\frac{\partial\theta}{\partial t}+\boldsymbol{u}\cdot\boldsymbol{\nabla}(z+\theta) = \nabla^2\theta, \tag{5.3}$$

where the Rayleigh number is defined by

$$R = \frac{g\beta\Delta T^2 d^3}{\nu K}. \tag{5.4}$$

The linear problem corresponding to (3.7) is

$$(\mathrm{D}^2-k^2)^3 f + 2R_0 k^2(1-z)f = 0, \tag{5.5}$$

where $f(z)$ now denotes the temperature fluctuation rather than the velocity. For the case of a stress-free boundary at $z = 0$ maintained at 0 °C with unbounded fluid above, a shooting method was applied to (5.5) to show that $k_c = 1.59$, $R_c = 275.4$.

The weakly nonlinear analysis was carried out in a similar manner to that described in §4. The values of E and F obtained were

$$E = -\frac{0.251}{\sigma^2}-\frac{0.245}{\sigma}+22.6, \tag{5.6}$$

$$F = \frac{1.03}{\sigma^2}+\frac{23.9}{\sigma}+97.7. \tag{5.7}$$

At high Prandtl number, both rolls and squares are subcritical ($E, F > 0$), so it is impossible to tell from the weakly nonlinear analysis which is preferred. At low Prandtl number however, squares are more likely to be observed since the roll solution becomes supercritical. The value of σ at which the roll solution changes from subcritical to supercritical is that for which $E = 0$, which is $\sigma = 0.11$. This result agrees well with computational work done by N. H. Brummell at Imperial College (personal communication).

The essential difference between the Veronis model and the 'S' model is that in the former, the curved density profile is caused by a nonlinear equation of state with a linear temperature profile, while in the latter it is produced by a linear equation of state and a nonlinear temperature profile. This means that the argument for the occurrence of a finite-amplitude instability in the Veronis model, where mixing maintains the temperature difference across the unstable layer while increasing its depth and hence the Rayleigh number (Moore & Weiss 1973), does not apply to the 'S' model, where mixing would tend to erode the cubic temperature profile, leading to a smaller temperature difference across the unstable layer.

To check that it is this difference between the two models that causes the qualitative difference in the results, rather than the fact that one of the models has a boundary, it is useful to consider a third model, in which a density profile identical with that of the Veronis model is produced by a linear equation of state and a quadratic temperature profile maintained by uniform internal heating. In this model, (5.5) is obtained, with f representing the vertical velocity, so the critical Rayleigh number is the same as for the Veronis model. The extent of overshooting in the main cell is different however, being up to $z = 2{\cdot}1$ compared with $z = 1.5$ for the Veronis model ($z = 1$ is the point of maximum density). The nonlinear behaviour is quite different, the equations analogous to (5.2) and (5.3) being

$$\frac{1}{\sigma}\left(\frac{\partial \boldsymbol{u}}{\partial t}+\boldsymbol{u}\cdot\nabla\boldsymbol{u}\right) = -\nabla P + R\theta\hat{\boldsymbol{z}}+\nabla^2\boldsymbol{u}, \tag{5.8}$$

$$\frac{\partial\theta}{\partial t}+\boldsymbol{u}\cdot\nabla(z^2-2z+\theta) = \nabla^2\theta. \tag{5.9}$$

The nonlinear analysis was repeated for this model, for rolls only, with the result that the bifurcation is always supercritical. Thus this model behaves more like the 'S' model than the Veronis model, so the subcritical behaviour of the Veronis model is indeed due to the use of a nonlinear equation of state.

6. Vertical asymmetry and the hexagonal planform

The 'S' model for penetrative convection considered up to now has had a rather artificial up–down symmetry. This forces the form of the evolution equations (4.11) to share that symmetry, leading to a symmetrical bifurcation. If the symmetry is broken then a transcritical bifurcation is possible for the asymmetric hexagonal planform given by

$$h(x,y) = A(\tau)\left[\cos(ky)+2\cos\left(\frac{\sqrt{3}kx}{2}\right)\cos(\tfrac{1}{2}ky)\right]. \tag{6.1}$$

With this loss of symmetry, the expansions for R and t become $R = R_c+\epsilon R_1,\ldots,$ $\tau = \epsilon t$. The solvability condition is then applied at second order in the expansion, giving

$$C\frac{\mathrm{d}A}{\mathrm{d}\tau} = DR_1A+GA^2, \tag{6.2}$$

where C and D are the same positive quantities as in (4.11) and G involves integrals of terms that are cubic in the first-order functions and their derivatives. For the symmetrical problem the first-order functions are even and $G = 0$. If $G > 0$, steady subcritical ($R_1 < 0$) solutions exist with $A > 0$, corresponding to 'up' hexagons, with the flow directed upwards at the centre of each hexagon. $G < 0$ allows subcritical 'down' hexagons.

The required asymmetry may easily be introduced in the boundary conditions. For the case of a stress-free boundary at $z = -1$, with unbounded fluid above, the solution to the linear problem is $k_c = 1.18$, $R_c = 76.4$, which was found using a shooting method for (3.7), and

$$G = 2.15-\frac{0.576}{\sigma}. \tag{6.3}$$

Thus at high Prandtl number, 'up' hexagons may occur subcritically, but for $\sigma < 0.268$, 'down' hexagons occur.

This analysis was repeated for a rigid boundary at $z = -1$, and for a stress-free boundary at $z = 0$, which also corresponds to the odd-mode solution of the original problem without boundaries. In each case the result was qualitatively the same, with 'up' hexagons at high Prandtl number and 'down' hexagons at low Prandtl number.

For Veronis' model of penetrative convection, which does not have vertical symmetry, a similar calculation shows that 'up' hexagons can occur subcritically for all values of the Prandtl number.

7. Discussion

The most interesting result of this work is that the bifurcation in our 'S' model of penetrative convection is supercritical. This means that weakly nonlinear theory can be used to predict the planform of convection near onset, with the result that rolls are preferred to squares. For the model studied by Veronis (1963), the bifurcation is subcritical, so the planform cannot be predicted, except at low Prandtl number, where squares are preferred because the roll solution becomes supercritical. The subcritical bifurcation of the Veronis model is caused by the use of a nonlinear equation of state. The results suggest that if penetrative convection is caused by a nonlinear equation of state, the bifurcation is subcritical, while if it is caused by a nonlinear temperature profile, the bifurcation is supercritical. The Veronis model should not therefore be applied to penetrative convection that is caused by a nonlinear temperature profile, for example convection in the ocean due to surface cooling at night, as it underestimates the extent of overshooting and introduces a finite-amplitude instability.

There are a number of reasons for caution when applying this work to ice-covered lakes. First, the results are only applicable for Rayleigh numbers close to critical, while in nature, Rayleigh numbers are often 10^6 or higher. Secondly, the model describes a simplified approximation to the temperature profiles produced in ice-covered lakes by the effect of solar heating (Matthews & Heaney 1987), particularly in its assumption of a steady state.

At higher Rayleigh numbers, the problem becomes meaningless as specified here, because the Rayleigh number given by (2.4) is not under experimental control since convection breaks down the temperature profile. A proper definition of the Rayleigh number would have to involve the strength of the internal heating function rather than the temperature difference in the unstable layer.

I am grateful to Dr T. J. Pedley, Dr P. F. Linden, Dr M. R. E. Proctor and Dr S. I. Heaney for their helpful criticism, and to the N.E.R.C. for financial support through the CASE studentship scheme.

REFERENCES

Azouni, M. A. 1983 Hysteresis loop in water between 0 and 4 °C. *Geophys. Astrophys. Fluid Dyn.* **24**, 137–142.

Jenkins, D. R. & Proctor, M. R. E. 1984 The transition from roll to square-cell solutions in Rayleigh–Bénard convection. *J. Fluid Mech.* **139**, 461–471.

Latour, J. & Zahn, M. P. 1978 On the boundary conditions imposed by a stratified fluid. *Geophys. Astrophys. Fluid Dyn.* **10**, 311–318.

MALKUS, W. V. R. 1960 Considerations on localized velocity fields in stellar atmospheres. In *Aerodynamic Phenomena in Stellar Atmospheres IAU Symp.* 12 (ed. R. N. Thomas), p. 346. Bologna: Zanichelli.

MATTHEWS, P. C. & HEANEY, S. I. 1987 Solar heating and its influence on mixing in ice-covered lakes. *Freshwater Biol.* **18**, 135–149.

MOORE, D. R. & WEISS, N. O. 1973 Nonlinear penetrative convection. *J. Fluid Mech.* **61**, 553–581.

VERONIS, G. 1963 Penetrative convection. *Astrophys. J.* **137**, 641–663.